Monolithic Nanostructured Silicate Family Templated by Lyotropic Liquid-Crystalline Nonionic Surfactant Mesophases

1 AUTHOR:

Sherif El-Safty

National Institute for Materials Science

168 PUBLICATIONS **3,146** CITATIONS

Monolithic Nanostructured Silicate Family Templated by Lyotropic Liquid-Crystalline Nonionic Surfactant Mesophases

S. A. El-Safty*

Chemistry Department, Faculty of Science, Tanta University, Tanta, Egypt

and

T. Hanaoka[†]

Tohoku Center, National Institute of Advanced Industrial Science and Technology (AIST), 4-2-1 Nigatake, Miyagino-ku, Sendai, 983-8551, Japan

A family of well-defined highly ordered mesoporous silica materials (designated as HOM) was synthesized by using a high concentration of nonionic amphiphile of Brij 56 surfactant ($C_{18}EO_{10}$) as a structure-directing species. Monolithic nanostructures with regular arrays and extended periodicity were produced under acidic conditions and different ambient temperatures (25−45 °C). Liquid-crystal phases formed in aqueous/silica domains played an important role in controlling the monolithic structural morphology. The direct templating method enhanced the phase topology of Brij 56 with three-dimensional (3-D) accessible mesoporous silica of primitive-centered cubic $Pn3m$ (HOM-7), 3-D hexagonal $P6_3/mmc$ (HOM-3), and solid phase (S) with cubic $Ia3d$ space group (HOM-5) mesophases. By adjustment of the phase behavior of Brij 56/TMOS mass ratio, ca. 35, 50, 70, and 75 wt %, the method yielded predictable mesophase structures of cubic spherical micellar $Im3m$ (HOM-1), 2-D hexagonal $P6mm$ (HOM-2), bicontinuous cubic $Ia3d$ (HOM-5), and lamellar L_∞ (HOM-6), respectively. A significant result was that the long-range ordered silica monoliths remained unchanged throughout the fast condensation of TMOS and removal of Brij 56 surfactant. Furthermore, all of the silica monoliths (HOM-types) had high surface area, uniform mesopore channels, well-defined morphological architectures, and large wall thickness of materials. HOM mesoporous molecular sieves were characterized by using powder X-ray diffraction, the Brunauer−Emmett−Teller method for nitrogen adsorption/desorption isotherms, transmission electron microscopy, and scanning electron microscopy. The results show that this direct template methodology can be used to successfully synthesize periodic mesoporous silica monoliths with a high degree of control over the mesopore morphology and the surfactant mesophase structures.

Introduction

Mesoporous molecular sieves have attracted much interest in recent years because of their potential applications in heterogeneous catalysis,[1−3] separation of biological molecules,[4−8] semiconductors,[9−11] and storage batteries.[12] Supramolecular arrays of organic amphiphiles are commonly used as structure-directing agents in the synthesis of mesoporous materials. The nature of inorganic precursors and the synthesis conditions crucially influence the quality of materials with desired nanoporous architectures. In 1992, the mesoporous silicates of three members of the M41S family, namely, MCM-41 (hexagonal $P6mm$), MCM-48 (cubic $Ia3d$), and MCM-50 (lamellar), were synthesized under basic conditions in the presence of ionic surfactants such as alkyltrimethylammonium bromide.[13,14] Furthermore,

* Corresponding author. Fax: +81-022-2375226. E-mail: Sherif.El-Safty@aist.go.jp or Saes682001@yahoo.co.uk.
† E-mail: hanaoka-takaaki@aist.go.jp.

(1) Corma, A. *Chem. Mater.* **1997,** *97,* 22373.
(2) Beck, J. S.; Vartuli, J. C. *Curr. Opin. Solid State Mater. Sci.* **1996,** *1,* 76.
(3) El-Safty, S. A.; Evans, J.; El-Sheikh, M. Y.; Zaki, A. B. *Colloids Surf. A* **2002,** *203,* 217.
(4) Kisler, J. M.; Dähler, A.; Stevens, G. W.; O'Connor, A. J. *Microporous Mesoporous Mater.* **2001,** *44,* 769.
(5) Grün, M.; Kruganoz, A. A.; Schacht, S.; Schüth, F. Unger, K. K. *J. Chromatogr. A* **1996,** *740,* 1.
(6) Sayari, A. *Stud. Surf. Sci. Catal.* **1996,** *102,* 1.
(7) Maschmeyer, T. *Curr. Opin. Solid State Mater. Sci.* **1998,** *3,* 71.
(8) Ying, J. Y.; Mehnert, C. P.; Wong, M. S. *Angew. Chem., Int. Ed.* **1999,** *38,* 56.

(9) Nandhakumar, I.; Elliott, J. M.; Attard, G. S. *Chem. Mater.* **2001,** *13,* 3840.
(10) Jin, C.; Luttmer, J. D.; Simth, D. M.; Ramos, T. A. *MRS Bull.* **1997,** *22,* 39.
(11) Yang, H.; Coombs, N.; Ozin, G. A. *Nature* **1997,** *386,* 692.
(12) Attard, G. S. *Macromol. Symp.* **2000,** *156,* 179.
(13) Kresge, C. T.; Leonowicz, M. E.; Roth, W. J.; Vartuli, J. C.; Beck, J. S. *Nature* **1992,** *359,* 710.
(14) Beck, J. S.; Vartuli, J. C.; Roth, W. J.; Leonowicz, M. E.; Kresge, C. T.; Schmitt, K. D.; Chu, C. T. W.; Olsan, D. H.; Higgins, E. W.; Schlenker, J. L. *J. Am. Chem. Soc.* **1992,** *114,* 10834.

under acidic conditions (pH ≤ 3), a wide range of nonionic surfactants with di- or triblock copolymers as templates were used to produce periodic mesoporous silicas such as SBA-1 and SBA-6 (*Pm3n*),[15–17] SBA-2 and SBA-12 (*P6₃/mmc*),[18] SBA-11 (*Pm3m*), and [18] SBA-16 (*Im3m*).[18,19] Under neutral conditions, nonionic surfactants were used to produce disordered mesoporous materials such as HMS,[20] MSU-*n*,[21] MSU-V,[22] and KIT.[23] In mild acidic solution (1 < pH < 4), poly-(ethylene oxide) surfactant was used as a template to produce ordered MSU-X mesoporous silica via a two-step pathway synthesis.[24,25] In those studies, mesoporous silica oxides were synthesized from micellar solutions with low surfactant concentrations. Mesoporous silicate oxides are formed via the charge density matching between amphiphilic assemblies and inorganic precursors.[26] Such interactions can significantly alter the phase behavior of surfactants and limit the ability to predict the mesophase topologies.

Potentially, direct templating by lyotropic liquid-crystal phases formed under relatively high surfactant concentration (≥30%) is a recognized method for achieving a high degree of control over the mesopore morphology and for preparing predictable large silicate monoliths compared with silicate powders prepared from micellar solution.[27,28] Nonionic alkyl poly(oxyethylene) surfactants, such as Brij types were used to prepare mesoporous silica monoliths in ordered structures similar to those of the M41S and SBA materials. Compared with ionic surfactants, Brij types are convenient as structure-directing agents because they are neutral, inexpensive, nontoxic, and biodegradable.[18] For example, Attard et al. produced three liquid-crystal phases by using nonionic surfactants as a template to produce nanoporous silica structures of these phases;[29,30] H₁-silica (hexagonal) was obtained by using $C_{16}EO_{10}$ as the surfactant,[29] whereas *Ia3d*-silica (cubic) and L∞-silica (lamellar) were obtained by using $C_{18}EO_8$.[30] Recently, by using lyotropic liquid-crystal mesophases of the surfactant Brij 76 ($C_{18}EO_{10}$), we synthesized a long-

Table 1. Experimental Synthesis Conditions for Preparation of Mesoporous Silica Monoliths (HOM-*n*)

HOM type	mesophase structure	*T* (°C)	composition mass ratio (w/w)			reaction time (min)
			Brij 56	TMOS	H₂O/HCl	
HOM-1	cubic *Im3m*	35	0.7	2	1	10
HOM-2	H₁ *P6mm*	35	1.0	2	1	10
HOM-3	3-D H₁ *P6₃/mmc*	45	1.36	2	1	10
HOM-5	cubic *Ia3d*	45	1.4	2	1	10
HOM-6	lamellar L∞	40	1.5	2	1	10
HOM-7	cubic *Pn3m*	40	1.7	2	1	10
HOM-5	solid cubic *Ia3d*	25	1.4	2	1	10–20

range ordered mesoporous silicate family that included hexagonal (H₁-SiO₂), lamellar (L∞-SiO₂), lamellar solid phase (S−SiO₂), cubic (*Ia3d*-SiO₂), cubic (*Im3m*-SiO₂), and 3-D hexagonal (*P6₃/mmc*-SiO₂) materials.[31] These materials were highly efficient in removing organic substances in aqueous solution without loss of well-defined mesopore architectures during the separation process.[32]

In our current study, we developed a fast and reliable method to synthesize highly ordered mesoporous silica (HOM) by direct templating using lyotropic liquid-crystal mesophases of Brij 56 ($C_{16}EO_{10}$). The synthetic materials demonstrated the practical application of this direct templating method for a high degree of control over the mesopore organizations and surfactant phase topologies. Our results also show that the fabrication of large silica monoliths of particles of desired size and shape with all phases is feasible. The method successfully yielded two unique 3-D accessible mesoporous silica structures, namely, primitive-centered cubic *Pn3m* (HOM-7) and cubic solid-phase S*₍Ia3d₎* (HOM-5), and yielded five periodic mesoporous molecular sieves, namely, body-centered *Im3m* (HOM-1), 3-D hexagonal *P6₃/mmc* (HOM-3), bicontinuous cubic *Ia3d* (HOM-5), 2-D hexagonal *P6mm* (HOM-2), and lamellar L∞ (HOM-6).

Experiment

Materials. All materials were analytical grade and used as purchased without further purification. Tetramethyl orthosilicate (TMOS) and poly(oxyethylene) Brij 56 surfactant, $C_{16}H_{33}(OCH_2CH_2)_{10}OH$ designated $C_{16}EO_{10}$, were purchased from Sigma-Aldrich Company Ltd. (USA).

Sample Syntheses. Seven mesoporous silica monoliths, including cubic (*Im3m*), 2-D hexagonal (*P6mm*), 3-D hexagonal (*P6₃/mmc*), cubic (*Ia3d*), cubic solid phase (S*₍Ia3d₎*), lamellar (L∞), and cubic (*Pn3m*) phases, were synthesized by adjusting the composition mass ratio of Brij 56:TMOS:HCl/H₂O and the temperature of the synthesis conditions as shown in Table 1. Homogeneous sol−gel synthesis was achieved by adding Brij 56 at the composition ratio shown in Table 1, to TMOS in a 100-cm³ round flask and then shaking at 50 °C for 5 min until homogeneous. The exothermic hydrolysis and condensation of TMOS occurred rapidly by addition of acidified aqueous solution of HCl (pH = 1.3) to this homogeneous solution. An isotropic liquid formed by the hydrolysis of TMOS in Brij56/H₂O domains. The methanol produced from this hydrolysis of TMOS was removed in vacuo at a specified temperature (Table 1). As the hydrolysis/condensation reactions continued during the evacuation, the liquid viscosity of the material increased, and the resulting optical gel-like material acquired the shape and size of the reaction vessel (Figure 1). After a 10-min

(15) Huo, Q.; Margolese, D. I.; Ciesla, U.; Demuth, D. G.; Feng, P. Y.; Gier, T. E.; Sieger, P.; Leon, R.; Petroff, P. M.; Schüth, F.; Stucky, G. D. *Chem. Mater.* **1994**, *6*, 1176.

(16) Sakamoto, Y.; Kaneda, M.; Terasaki, O.; Zhao, D. Y.; Kim. J. M.; Stucky, G. D.; Shin, H. J.; Ryoo, R. *Nature* **2000**, *408*, 449.

(17) Huo, Q.; Leon, R.; Petroff, P. M.; Stucky, G. D. *Science* **1995**, *268*, 1324.

(18) Zhao, D.; Huo, Q.; Jianglin, F.; Chmelka, B. F.; Stucky, G. D. *J. Am. Chem. Soc.* **1998**, *120*, 6024.

(19) Kim, J. M.; Stucky, G. D. *Chem. Commun.* **2000**, 1159.

(20) Tanev, P. T.; Pinnavaia, T. J. *Science* **1995**, *267*, 865.

(21) Bagshaw, S. A.; Prouzet, E.; Pinnavaia, T. J. *Science* **1995**, *269*, 1242.

(22) Kim, S. S.; Zheng, W.; Pinnavaia, T. J. *Science* **1998**, *282*, 1302.

(23) Ryoo, R.; Kim, J. M.; Shin, C. H.; Lee, J. Y. *Stud. Surf. Sci. Catal.* **1996**, *105* A, 45.

(24) Boissiére, C.; van der Lee, A.; El Mansouri, A.; Larbot, A.; Prouzet, E. *Chem. Commun.* **1999**, *20*, 2047.

(25) Boissiére, C.; Larbot, A.; Bourgaux, C.; Prouzet, E.; Bunton, C. A. *Chem. Mater.* **2001**, *13*, 3580.

(26) Monnier, A.; Schüth, F.; Huo, Q.; Kumar, D.; Margolese, D.; Maxwell, R. S.; Stucky, G. D.; Krishnamurty, M.; Petroff, P.; Firouzi, A.; Janicke, M.; Chmelka, B. F. *Science* **1993**, *261*, 1299.

(27) Attard, G. S.; Glyde, J. C.; Göltner, C. G. *Nature* **1995**, *378*, 366.

(28) Campbell, T.; Corker, J. M.; Dent, A. J.; El-Safty, S. A.; Evans, J.; Fiddy, S. G.; Newton, M. A.; Ship, C. P.; Turin, S. *Stud. Surf. Sci. Catal.* **2001**, *132*, 667.

(29) Coleman, N. R. B.; Attard, G. S. *Microporous Mesoporous Mater.* **2001**, *44*, 73.

(30) Attard, G. S.; Edgar, M.; Göltner, C. G. *Acta Mater.* **1998**, *46*, 751.

(31) El-Safty, S. A.; Evans, J. *J. Mater. Chem.* **2002**, *12*, 117.

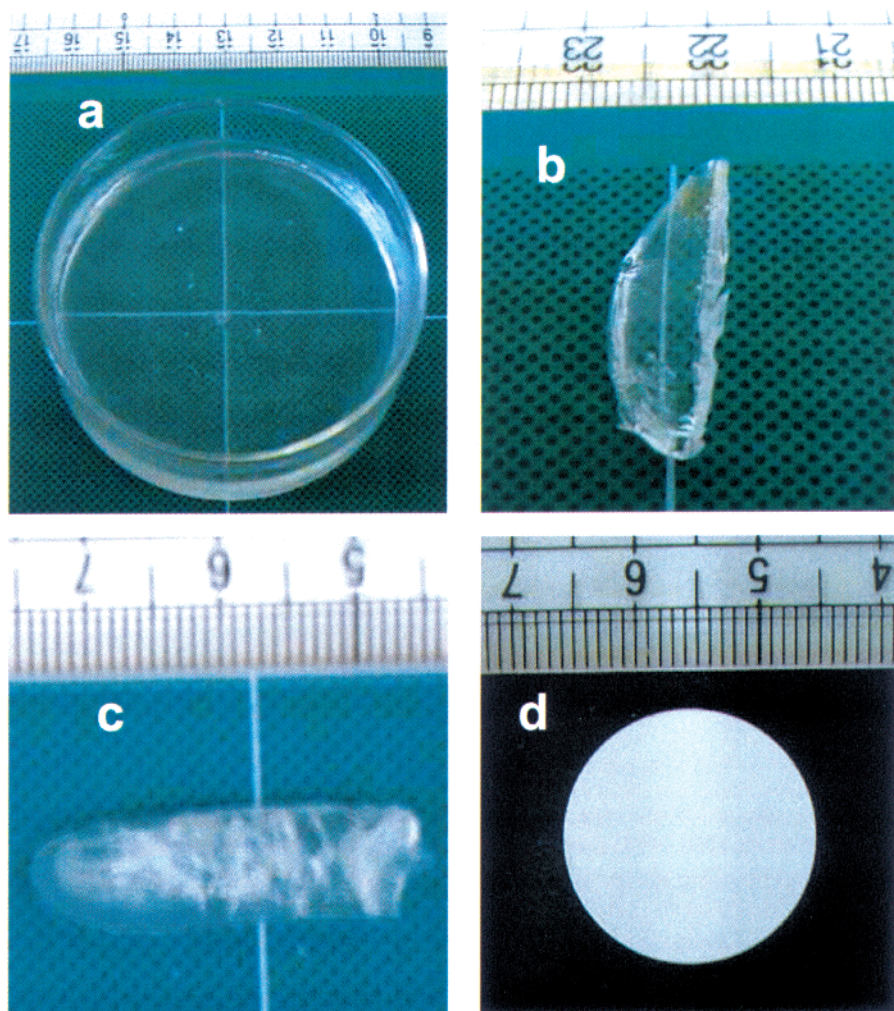(32) El-Safty, S. A. *J. Colloid Interface Sci.* **2003**, *260*, 184.

Figure 1. Optically translucent HOM silica monoliths: (a) as-synthesized monolithic silica-Brij 56 mesophase, (b) after drying and surfactant removal by ethanol extraction, (c) after removal of surfactant by calcination at 450 °C, and (d) formed as a compacted disk by grinding the sample into powder after calcination.

evacuation, the translucent glassy monoliths were collected and kept at 40 °C for 16 h. The surfactant was removed by calcination at 450 °C (3 h under nitrogen and 14 h under oxygen).

Analyses. Powder X-ray diffraction (XRD) patterns were measured by using a MXP 18 diffractometer (Mac Science Co. Ltd.) with monochromatic Cu Kα radiation. Nitrogen adsorption−desorption isotherms were measured at 77 K, and surface area measurements were determined by using the Brunauer−Emmett−Teller (BET) method, the data being collected with a Shimadzu ASAP 2020 surface area analyzer. Transmission electron microscopy (TEM) images were recorded by using a JEOL JEM-2000 FXII operating at an acceleration voltage of 200 kV. Scanning electron microscopy (SEM) micrographs were obtained by using a JEOL JSM-5600 operated at 7 keV.

Results and Discussion

1. HOM-*n* Silica Mesophase Formation Mechanism. The surfactant molecule (Brij 56) is capable of self-assembling into lyotropic phases in solution. However, the structure phase assemblies of Brij 56 contain cubic (I), hexagonal (H_I), cubic (V_1), and lamellar (L_∞, L_2).[29,33] The type of structure formed (Table 1) is determined by the surfactant molecule packing.[33] The liquid-crystal phase behavior of Brij 56 is influenced by

the choice of the composition ratio of Brij 56/TMOS and by the temperature and pH of the solution during the synthesis of mesoporous silica materials.[29,33] In this study, the mesoporous silica phases, which did not exist in the phase diagram of the Brij 56/H_2O system, were synthesized, including HOM-3 (3-D hexagonal $P63/mmc$), HOM-5 (cubic $Ia3d$ solid phase), and HOM-7 (cubic $Pn3m$). The synthetic nature of these unpredicted 3-D monoliths established that the TMOS/Brij 56 interactions can effectively change the value of the critical packing parameter of Brij 56 according to the mesophase geometrical shape formed.

In the preparation of HOM-*n* silica monoliths, TMOS hydrolyzes at low pH (∼1) to form positively charged protonated silica species ($\equiv Si(OH_2)^+$) and methanol. These silica species are only an intermediate species in the formation of siloxane Si−O−Si by further condensation.[18] As the hydrolysis and condensation continue, viscous gel-like materials are formed. The hydrophilic (EO) units of the Brij 56 surfactant ($C_{16}EO_{10}$) in the lyotropic phase interact with silica intermediate species through hydrogen-bonding or weak electrostatic interactions to promote the self-assembly of the silica-mesophase gel monoliths. Even in the absence of the strong interaction between surfactant and silica oligo-

(33) Mitchell, D. J.; Tiddy, G. J. T.; Waring, L.; Bostock, T.; McDonald, M. P. *J. Chem. Soc., Faraday Trans. 1* **1983**, *79*, 975.
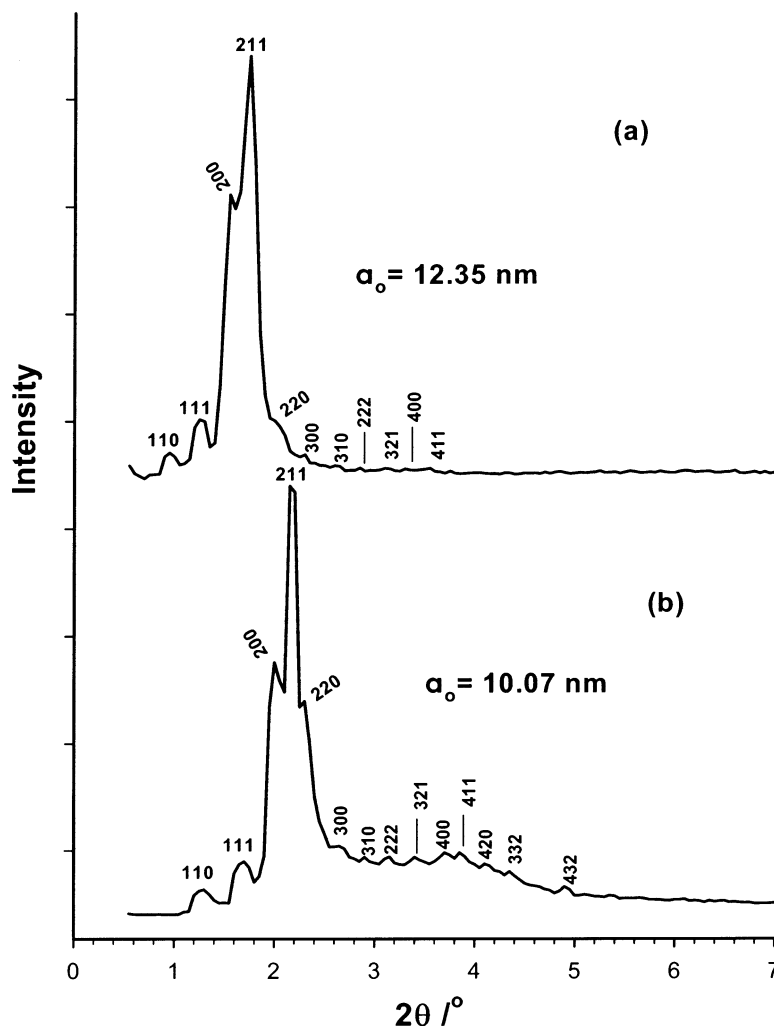
Figure 2. Powder X-ray diffraction patterns of the cubic *Pn*3*m* monolithic silicate: (a) as-synthesized and (b) calcined HOM-7 structures.

mers, large monoliths can be fabricated because fabrication does not depend on the type of interaction or on the surfactant structural charge. However, the use of a high concentration of the surfactant permits the pre-existence of the liquid-crystal phases that direct the formation of the architecture of inorganic mesophase silicates through the true liquid-crystal template mechanism.

The addition of HCl as a condensation catalyst to the Brij 56/TMOS/H$_2$O phase domains apparently assisted the performance of the gel precipitate (Figure 1) throughout the fast condensation process without loss of long-range ordered mesophase architectures. The inorganic precursor did not precipitate out of the synthesis solution mixture (Brij 56/ H$_2$O), suggesting that the gel-like materials acquire the size and shape of the reaction vessel, as clearly seen in Figure 1a. Methanol produced within the hydrolysis and condensation of TMOS destroys the liquid-crystal mesophases.[27,30] The evacuation of the methanol from the anisotropic mixture yielded the optically transparent monolithic gel, indicating the restoration of the original liquid-crystal mesophase. The translucent liquid-crystal phases remained unchanged during the drying and during the removal of the surfactant (Figure 1b,c). The key result is that HOM silica monoliths were fabricated as a compacted disk by grinding after calcination (Figure 1d), demonstrating

the feasibility of using HOM monoliths in practical applications.[4-8]

2. Characteristics of HOM-*n* Mesophase Structures. *2.1. Pn3m Cubic Structure (HOM-7).* The XRD patterns of HOM-7 (Figure 2) reveal the formation of the unique primitive-centered cubic *Pn*3*m* mesoporous silica. With a slightly higher concentration of Brij 56 (85 wt %), silica monoliths were successfully fabricated in 10 min at 40 °C. The small-angle XRD pattern for the as-synthesized mesoporous silica (Figure 2a) shows five well-resolved lines in the region $0.5 \leq 2\theta \leq 2°$, which were assigned to the (110), (111), (200), (211), and (220) reflections. This diffraction pattern is associated with primitive cubic lattice *Pn*3*m* symmetry.[34] The unique additional weak peaks in the $2 \leq 2\theta \leq 4°$ were respectively assigned to the (300), (310), (222), (321), and (411) reflections. The high-intensity (211) peak can be ascribed to a large unit-cell parameter ($a_o = d_{211}\sqrt{6}$ = 12.35 nm). The XRD results indicated that the as-synthesized cubic *Pn*3*m* mesophase (HOM-7) has a high degree of mesoscopic morphology of cubic lattice.

The XRD pattern of the HOM-7 silica after calcination (Figure 2b) shows that the HOM-7 (primitive cubic *Pn*3*m*) structure was a dominant phase, indicating the

(34) Honma, I.; Zhou, H. S.; Kundu, D.; Endo, A. *Adv. Mater.* **2000**, *12*, 1529.

thermal stability of cubic $Pn3m$ networks. Typically, all the diffraction peaks appeared at high intensity with slightly large 2θ values. The bulk resolved peaks were clearly evident with d spacing ratios of $\sqrt{2}:\sqrt{3}:\sqrt{4}:\sqrt{6}:\sqrt{8}:\sqrt{9}:\sqrt{10}:\sqrt{12}:\sqrt{14}:\sqrt{16}:\sqrt{18}:\sqrt{20}:\sqrt{22}:\sqrt{29}$, which are indicative of the high crystallinity of HOM-7 (cubic $Pn3m$) structures. We checked that the plot of reciprocal d spacings $(1/d_{hkl})$ of the observed reflections vs a function of $(h^2 + k^2 + l^2)^{1/2}$ follows a straight line with slope $= 1/\alpha$, where α is a predictable unit-cell dimension of ca. 9.8 nm,[35] which is a value consistent with the measured value ($\alpha_o = d_{211}\sqrt{6} = 10.07$ nm) of calcined cubic $Pn3m$ structure. In a previous study, Brij 56 surfactant was successfully used to yield (SBA-11) cubic $Pm3m$ mesoporous phase.[18] Our results here suggest that cubic $Pn3m$ (HOM-7) can be fabricated by using a high concentration of Brij 56/TMOS ratio (>0.8) under slightly acidic synthesis conditions.

Our results show that HOM-7 silica monoliths with primitive-centered cubic $Pn3m$ space symmetry had highly ordered 3-D network channels along the [100], [111], and [110] projections (Figure 3). The TEM micrograph of calcined material along the [100] zone axis (Figure 3a) shows square lattice particles with uniform pore arrays along this direction, reflecting the cubic $Pn3m$ symmetry. The estimated interplane spacing was about 40 Å, consistent with the high intensity of the d_{211} peak in the XRD pattern (Figure 2b). Therefore, the estimated unit-cell parameter was 9.8 nm, agreeing well with XRD data. The [111] projection exhibited diverse, yet uniform, channels in the cubic $Pn3m$ structure (Figure 3b). The TEM images along the [111] (Figure 3b) and [110] (Figure 3c) directions show well-ordered straight arrays. The TEM images provide good evidence of previously unreported highly three-dimensional HOM-7 (cubic $Pn3m$) network architectures.[31,36]

2.2. Ia3d Cubic Structure (HOM-5). Cubic $Ia3d$ structure with solid phase was successfully fabricated under the synthesis conditions listed in Table 1, despite the fact that the low condensation rate of TMOS accompanying the fabrication of the silica network matrix inhibited the solidification of the phase into clear optically anisotropic monoliths and that the surfactant characteristic of the solid phase led to the formation of lower curved aggregates arranged in the short-range order lamellar L_2 or L_∞ phase.[31,33] This liquid-crystalline order formed might be due to the effectiveness of the Brij 56 structure (hydrophobic, C_{16}-alkyl chain, and hydrophilic (EO_{10}) block lengths) in stabilizing the high surface curvature aggregates arranged in cubic $Ia3d$ solid phase. Figure 4a shows the low-angle XRD pattern for the liquid-crystal solid phase of the Brij 56 template (70 wt %). The XRD pattern shows well-resolved reflection peaks with d spacing ratios of $\sqrt{6}:\sqrt{8}:\sqrt{14}:\sqrt{16}:\sqrt{20}:\sqrt{22}:\sqrt{24}:\sqrt{26}:\sqrt{30}:\sqrt{32}$, respectively assigned to the (211), (220), (321), (400), (420), (332), (422), (431), (521), (440) reflections.[37–39] This XRD data of solid mesophase
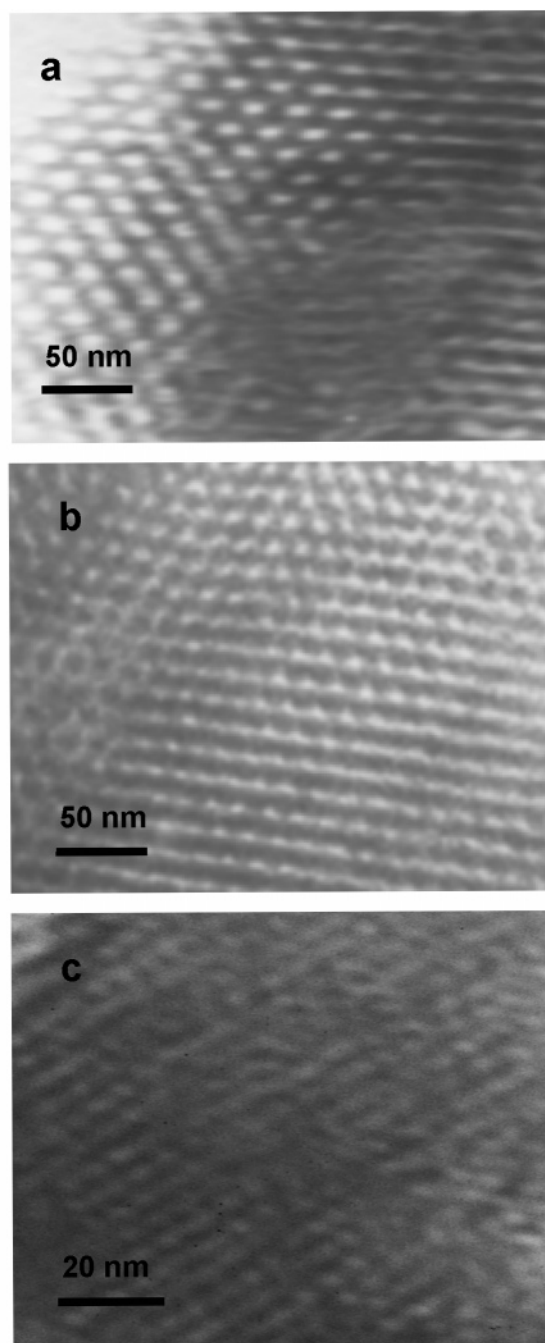

Figure 3. TEM images of calcined HOM-7 (cubic $Pn3m$) monolithic silica viewed along the (a) [100], (b) [111], and (c) [110] directions.

liquid crystal of Brij 56 (HOM-5) indicates highly ordered structures for the cubic crystallographic space group $Ia3d$, with a large unit-cell dimension of 10.6 nm. Furthermore, high-quality bicontinuous cubic $Ia3d$ mesophase (HOM-5) with a lattice constant parameter of ca. 10.4 nm was also successfully fabricated using the conditions of normal phase topology (V_1) listed in Table 1.[33] Well-resolved XRD planes with additional peaks were observed rather than planes of cubic S_{Ia3d}, particularly at high 2θ value (>4.5°). These peaks had d-spacing ratios of $\sqrt{38}:\sqrt{42}:\sqrt{46}:\sqrt{50}$, which were assigned to (611), (541), (631), (543). These XRD data

(35) Mariani, P.; Luzzati, V.; Delacroix, H. *J. Mol. Biol.* **1988**, *204*, 165.

(36) Lu, Y.; Ganguli, R.; Drewien, C. A.; Anderson, M. T.; Brinker, C. J.; Gong, W.; Guo, Y.; Soyes, H.; Dunn, B.; Huang, M. H.; Zink, J. I. *Nature* **1997**, *389*, 364.

(37) Romero, A. A.; Alba, M. D.; Klinowski, J. *J. Phys. Chem. B* **1998**, *102*, 123.

(38) Huo, Q.; Margolese, D. I.; Stucky, G. D. *Chem. Mater.* **1996**, *8*, 1147.

(39) Yu, C.; Yu, Y.; Miao, L.; Zhao, D. *Microporous Mesoporous Mater.* **2001**, *44*, 65.
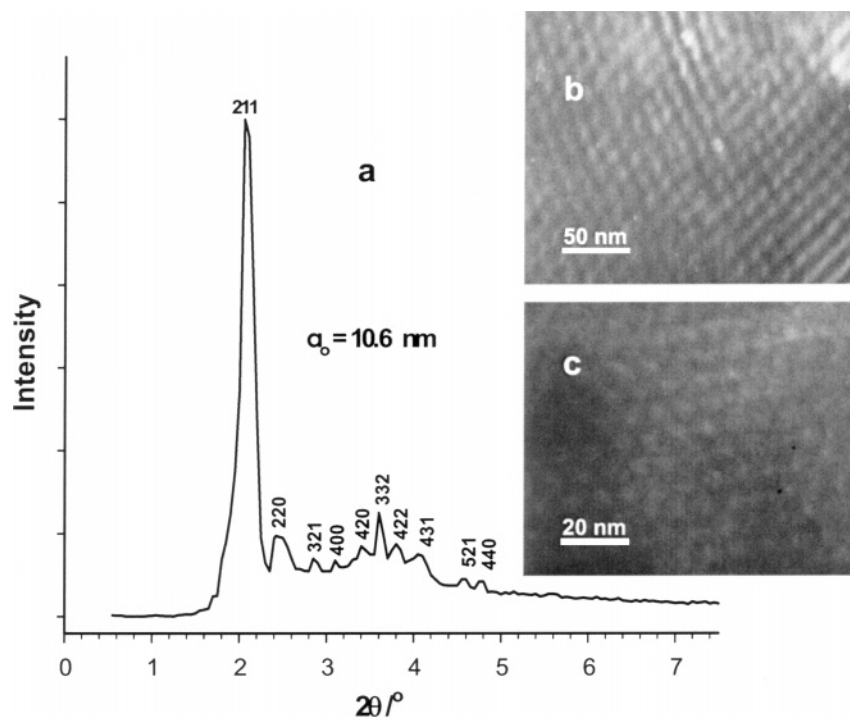
Figure 4. (a) Powder X-ray diffraction pattern of calcined HOM-5 (cubic solid-phase S_{Ia3d}) monolithic silicates. TEM images along the (c) [110] and (d) [100] directions for calcined HOM-5 in solid-phase S_{Ia3d} and normal bicontinuous topology.
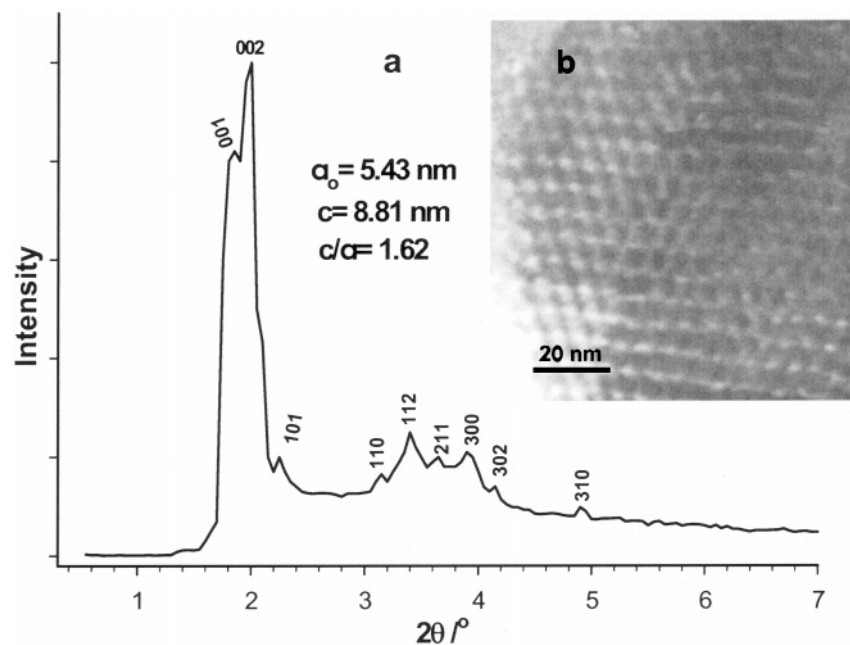

Figure 5. (a) Powder X-ray diffraction pattern of calcined HOM-3 (3-D hexagonal $P6_3/mmc$) monoliths and (b) TEM image along the [$\bar{1}2\bar{1}3$] zone axis for HOM-3 mesophase.

reflect the formation of a pure cubic $Ia3d$ mesoporous silicate with a high degree of crystalline structures that are similar to structures previously observed by using CTAB-types in MCM-48 mesoporous silicas.[14,37] Our TEM images of HOM-5 cubic ($Ia3d$) synthesized with solid-phase (S) and normal-phase topology (V_1) suggest the existence of 3-D ordered structures. The selected view of particles along the [110] (Figure 4b) and [100] (Figure 4c) directions showed well-defined, regular channels.

2.3. $P6_3/mmc$ 3-D Hexagonal Structure (HOM-3). XRD patterns (Figure 5a) reveal 3-D hexagonal $P6_3/mmc$ silica nanostructures (HOM-3) derived from a hexagonal close-packing parameter of as-synthesized Brij56/TMOS mesoporous arrays. The cell parameter ratio c/a_0 was 1.628 ($a_0 = 5.43$, $c = 8.81$ nm), which is considered an ideal ratio for a typical hexagonal close-packed (hcp) structure.[18,19] Clearly evident in the XRD patterns between $1 \leq 2\theta \leq 6°$ are nine peaks, which can be respectively assigned to (100), (002), (101), (110),
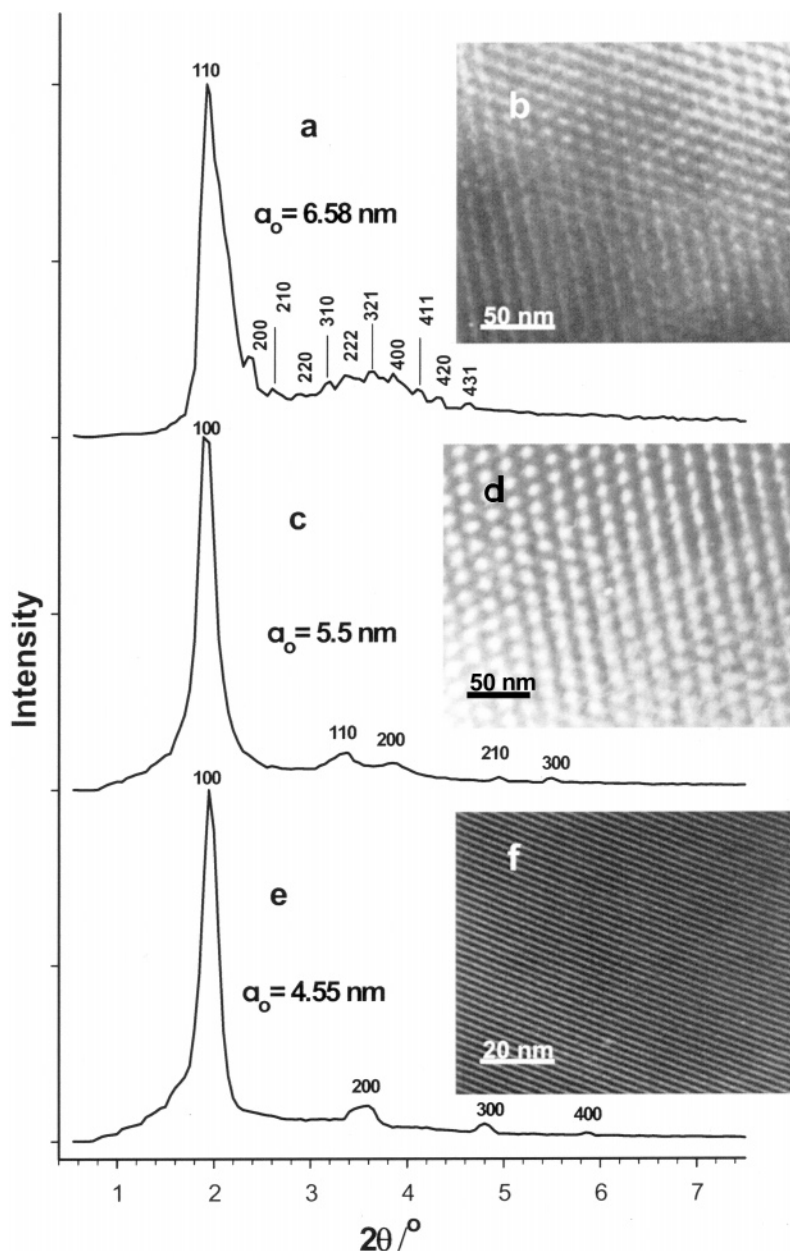
Figure 6. Powder X-ray diffraction patterns of the calcined silica monoliths (a) HOM-1 (cubic *Im*3*m*), (c) HOM-2 (hexagonal *P*6*mm*), and (e) HOM-6 (lamellar L∞). Representative TEM images of mesoporous silicates (b) HOM-1 (cubic *Im*3*m*), (d) HOM-2 (hexagonal *P*6*mm*), and (f) HOM-6 (lamellar L∞).

(112), (211), (300), (302), and (310) reflections of a 3-D hexagonal with a *P*6₃/*mmc* space group.[19] Previous studies report that the influence of the chain length structures of Brij 76 on the formation of the more curved aggregates arranged in 3-D hexagonal is stronger than that of Brij 56.[18] Therefore, a 3-D hexagonal *P*6₃/*mmc* structure was not previously defined by other synthesis routes using Brij 56 surfactant, indicating the high degree of control by using the liquid-crystal templating method over the 3-D hexagonal mesophase structures. The XRD reflections of HOM-3 prepared from liquid-crystal phase of Brij 56 (Figure 5a) are clearly assigned to the better ordered channels and higher uniform textures of the 3-D hexagonal *P*6₃/*mmc* materials, compared with the channels and textures of SBA-12 mesoporous silicas prepared by using Brij 76 as previously reported.[18,31] The TEM image of the HOM-3 silica monoliths along the [$\bar{1}2\bar{1}3$] zone axis (Figure 5b) clearly

reveals well-ordered channels arranged in hexagonal close-packed layers.[17]

2.4. Im3m Cubic Structure (HOM-1). Cubic mesoporous silica with *Im*3*m* (HOM-1) was synthesized by using Brij 56 species at a lower temperature (35 °C) and Brij 56/TMOS composition ratio of 35 wt %, compared with that by using Brij 76 species,[31] indicating the easy preparation of cubic *Im*3*m* phase by using Brij 56 as the template. XRD patterns (Figure 6) reveal the high periodicity and regularity of mesoporous HOM-1 and show finely resolved Bragg's diffraction peaks with *d*-spacing ratios of $\sqrt{2}$:$\sqrt{4}$:$\sqrt{6}$:$\sqrt{8}$:$\sqrt{10}$:$\sqrt{12}$:$\sqrt{14}$:$\sqrt{16}$:$\sqrt{18}$:$\sqrt{20}$:$\sqrt{26}$, which can be respectively assigned to (110), (200), (211), (220), (310), (222), (321), (400), (411), (420), (431) reflections. The presence of all important XRD diffraction peaks of cubic *Im*3*m* symmetry with $\alpha_0 = 6.58$ nm (Figure 6a) indicate a high degree of ordering of the 3-D channels of large caged cubic *Im*3*m*

Monolithic Nanostructured Silicate Family

Chem. Mater., Vol. 15, No. 15, 2003 **2899**

structures (HOM-1).[39] The TEM micrograph (Figure 6b) reveals high-quality mesoporous structures. The view along the [100] direction shows regular cubic *Im*3*m* mesoporous silicate (HOM-1) with uniform 3-D channels (Figure 6b).[32,40]

2.5. 2-D Hexagonal P6mm (HOM-2) and Lamellar (HOM-6) Structures. HOM-2 (2-D hexagonal *P*6*mm*) and HOM-6 (bilayered lamellar L_∞) mesophases were successfully synthesized by using Brij 56 species at 35 and 40 °C, respectively, consistent with structures synthesized by using the same composition ratio of Brij76/ TMOS (25 °C) previously reported.[29,31] The XRD patterns (Figure 6c) show five well-ordered peaks that can be respectively assigned to (100), (110), (200), (210), and (300) reflections. The synthesized mesoporous molecular sieves (HOM-2) at 50 wt % of Brij 56 are consistent with *P*6*mm* hexagonal symmetry analogous to highly ordered mesoporous MCM-41 and to SBA-15.[13–15] Anderson et al. similarly synthesized MCM-41 silica monoliths by using TMOS and CTAB as structure-directing species.[41] The high-intensity (100) peak (Figure 6c) shows a *d* spacing of 4.7 nm, corresponding to a unit-cell dimension of $\alpha_o = 2d_{100}/\sqrt{3} = 5.5$ nm. The presence of resolved XRD peaks reflects excellent structural order extended over a long range of the cylindrical mesopore hexagonal arrays.[42] The TEM image (Figure 6d) reveals a well-defined hexagonal lattice with regular arrays along the [100] projection. The regularity of the spots in the image corresponds to the channels running along this direction.[43] The TEM image of HOM-2 silica reveals 2-D *P*6*mm* hexagonal symmetry. The estimated separation distance between the channels was 4.4 nm, which agrees well with the d_{100} spacing observed in the XRD reflection planes (Figure 6c).

Figure 6e shows the XRD patterns of the calcined lamellar structure prepared at 75 wt % Brij 56/TMOS and at 40 °C. The four well-resolved diffraction peaks correspond to the (100), (200), (300), and (400) planes of highly ordered lamellar mesophase materials (HOM-6).[13] Previous reports show that MCM-50 mesoporous silicas synthesized using cationic surfactant CTAB or nonionic diblock copolymer as templates often collapse after the calcination.[14,39] Additionally, even at higher composition ratios of Brij 56/silica (>0.6), poorly ordered, unstable lamellar-like mesophase was formed,[18] indicating that the direct templating method produces substantial stability in the lamellar structures after calcination.[27,31] The TEM image of the HOM-6 mesophase silicate monoliths (Figure 6f) clearly reveals highly ordered layers of lamellae phase.[44] The interlayer distance of the lamellar sample was about 4.3 nm, which is consistent with the d_{100} X-ray reflection peak.

2.6. Mesostructured Particle Morphology. The SEM micrographs of the mesophase samples (Figures 7 and 8) reveal large particle morphologies (ca. 5–10-μm long) with crystal structures of various sizes and shapes. The SEM micrographs show that all of the mesophases
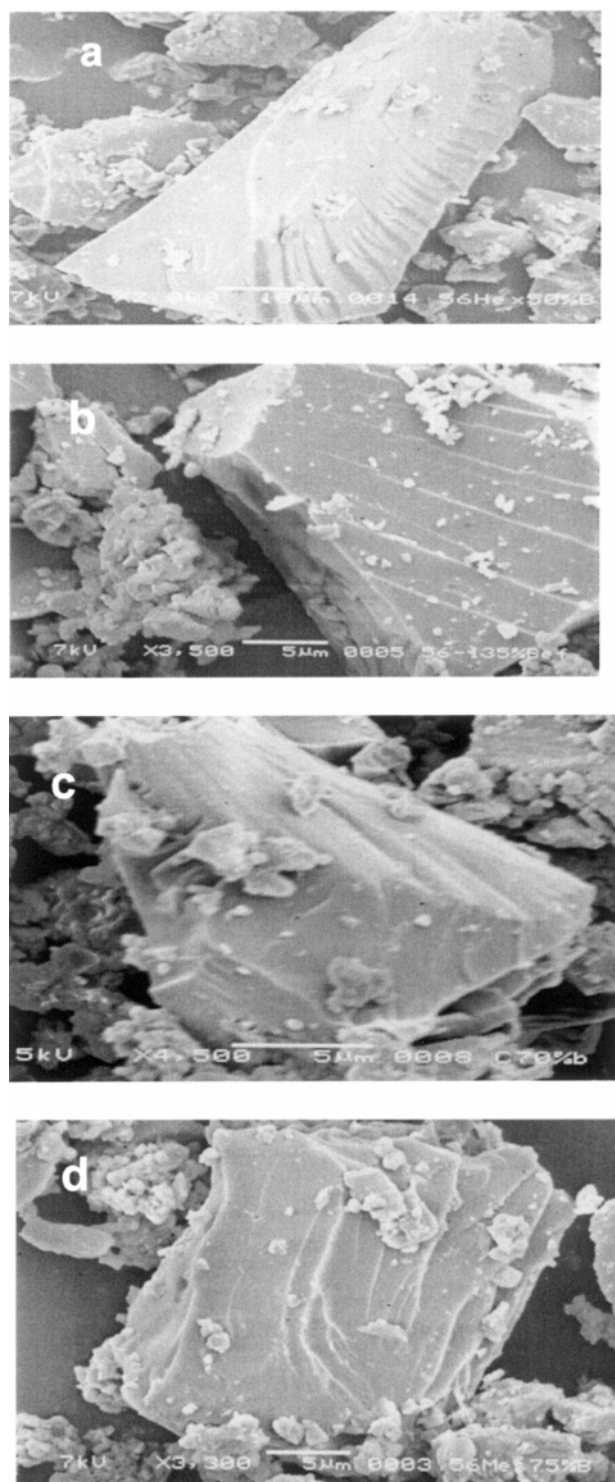
Figure 7. SEM images of particle morphologies for (a) HOM-2 (hexagonal *P*6*mm*), (b) HOM-1 (cubic *Im*3*m*), (c) HOM-5 (cubic *Ia*3*d*), and (d) HOM-6 (lamellar L_∞).

exhibited three significant features. First, the surface architecture was quite smooth, suggesting high crystallinity of HOM mesoporous silica materials.[45] Second, porous particles had platelike or roselike shaped morphology.[46] Third, all of the structures, regardless of size or shape, showed well-defined strip lines, which might be an indicator of interior long-range channels.

(40) Zhao, D.; Yang, P.; Melosh, N.; Jianglin, F.; Chmelka, B. F.; Stucky, G. D. *Adv. Mater.* **1998**, *10*, 1380.

(41) Anderson, M. T.; Martin, J. E.; Odinek, J. G.; Newcomer, P. P.; Wilcoxon, J. P. *Microporous Mater.* **1997**, *10*, 13.

(42) Zhao, D.; Jianglin, F.; Huo, Q.; Melosh, N.; Fredrickson, G. H.; Chmelka, B. F.; Stucky, G. D. *Science* **1998**, *279*, 548.

(43) Alfredsson, V.; Anderson, M. W.; Ohsuna, T.; Terasaki, O., Jacob, M.; Bojrup, M. *Chem. Mater.* **1997**, *9*, 2066.

(44) Ayyappan, S.; Rao, C. N. R. *Chem. Commun.* **1997**, 575.

(45) Khimyak, Y. Z.; Klinowski, J. *Chem. Mater.* **1998**, *10*, 2258.

(46) Reid, B. D.; Trevino, A. R.; Musselman, I. H.; Balkus, K. J.; Ferraris, J. P. *Chem. Mater.* **2001**, *13*, 2366.
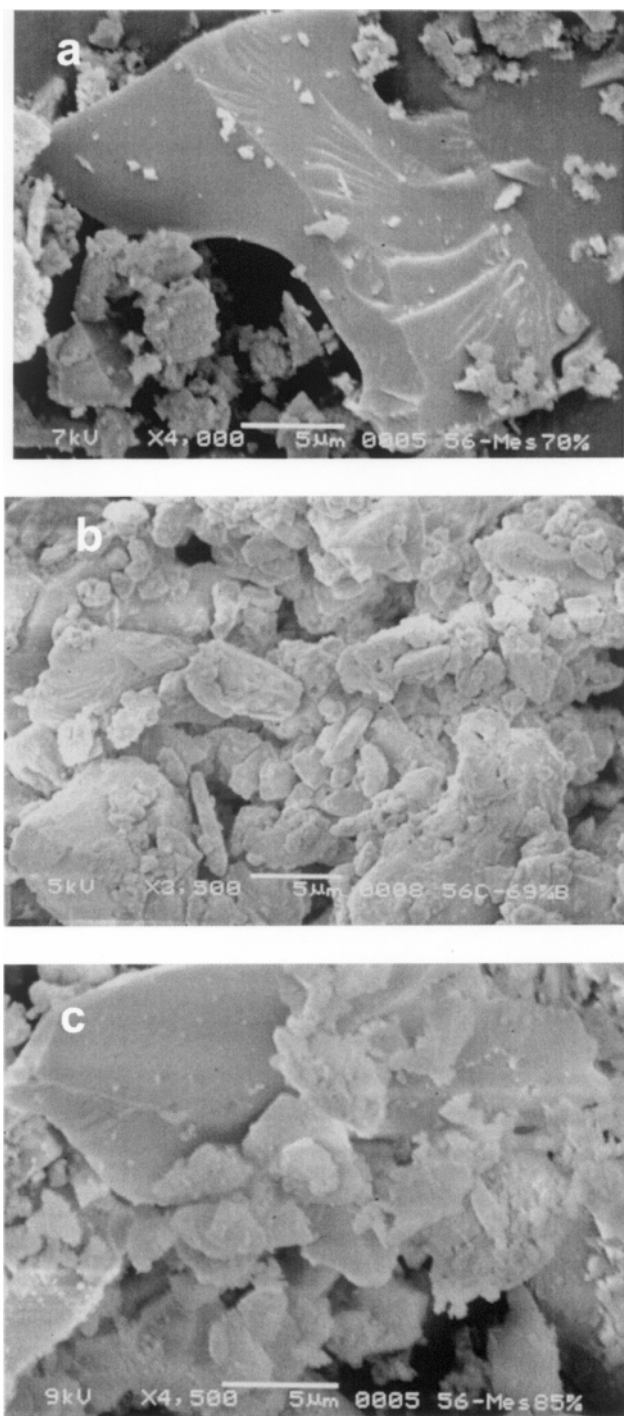
Figure 8. SEM images of particle morphologies for (a) HOM-4 (cubic *Ia3d* solid phase), (b) HOM-3 (3-D hexagonal *P6₃/mmc*), and (c) HOM-7 (cubic *Pn3m*).

The SEM images of the 3-D architectures (Figure 8) of cubic *Ia3d* solid phase (HOM-4), 3-D hexagonal *P6₃/mmc* (HOM-3), and cubic *Pn3m* (HOM-7) show a high degree of crystallinity and are similar to the architecture observed in microporous crystalline zeolites.[47] The range of different surface textures of the large monolith particles (Figure 8) produced by using the direct templating methodology reflect additional control over the nanostructure morphology.

2.7. N₂ Adsorption/Desorption Isotherms. Figure 9 shows the N₂ adsorption/desorption isotherms for calcined HOM mesoporous molecular sieves. All the mesoporous silicates exhibited typical reversible type-IV adsorption isotherms as defined by IUPAC.[48] Adsorption at low P/P_o (<0.3) occurs via monolayer−multilayer adsorption of N₂ on the wall of the mesopores. At $0.3 \leq P/P_o \leq 0.5$, the isotherms exhibited a sharp inflection characteristic of capillary condensation within uniform mesopores; the specific P/P_o position of the inflection point depended on the type of mesophase material. The sharpness in this inflection point suggests the uniformity of the pore size distribution system.[49] Neither the HOM-1 (cubic *Im3m*) or HOM-2 (hexagonal *P6mm*) mesoporous silicates (Figure 9a,b) showed any defined hysteresis loop in their adsorption/desorption isotherms, possibly due to no blocking (network effects) of narrow pores, indicating a highly uniform pore size of HOM-*n* materials.[3,27] The pore condensation of HOM types synthesized with a slightly higher concentration of Brij 56 (69−85 wt %) was characterized by a small H₂-type hysteresis loop (Figure 9c,d) typical of small mesopores of ∼3 nm, in contrast to that of MCM-41.[14] Such H₂-type hysteresis loops occurred at $P/P_o > 0.4$, in which materials showed relatively uniform channel-like or bottle-shaped pores.[50] The width of the hysteresis loop of the sorption isotherms decreased with decreasing pore width, as similarly reported for MCM-48 and MCM-41 mesoporous silicates.[51]

The total pore volume *V* of a given material (Table 2) can be calculated from the N₂ amount adsorbed at P/P_o close to the saturation vapor pressure ($P/P_o = 0.97$). This *V* reflects the volume of the HOM-*n* pores in which capillary condensation and micropore filling occurred plus the adsorbed volume on the surface of the pores. The calculated *V* ranged from 0.5 to 0.84 cm³/g, similar to the volume of uniform pores reported for a purely siliceous highly ordered M41S.[14,51] The large BET surface area is indicative of uniform framework-confined channels of mesoporous silica.[50] The calculated *V* and surface area S_{BET} (Table 2) increased with increasing composition ratio of Brij 56/TMOS in the synthesis of HOM-*n* materials.

The pore size distribution of calcined mesoporous silicates was obtained from the desorption data (Figure 9) by using the Barrett−Joyner−Halenda (BJH) formula.[52] The BJH plot for the N₂ physisorption on the mesoporous silicate family reveals a uniform pore size distribution, which is relatively independent of the different HOM-*n* phases. It might be attributed to the pore size in the accessible range of hydrophobic (C₁₆-hydrocarbon chain) and hydrophilic (EO₁₀) block lengths of Brij 56, which provide pore sizes in the range of 3−3.5 nm in diameter (Table 2). When Brij 76 was used as a template, the pore size ranged between 3.4 and 3.9 nm, indicating the effect of the block lengths of the surfactant aggregate on the pore size.[31] The approximate pore

(47) Balkus, K. J.; Godefroy, G.; Deng, Z. *Microporous Mesoporous Mater.* **2002**, *52*, 141.

(48) Brunauer, S.; Deming, L. S.; Deming, W. S.; Teller, E. *J. Am. Chem. Soc.* **1940**, *62*, 1723.
(49) Evans, J.; Zaki, A. B.; El-Sheikh, M. Y.; El-Safty, S. A. *J. Phys. Chem. B* **2000**, *104*, 10271.
(50) Kruk, M.; Jaroniec, M. *Chem. Mater.* **2001**, *13*, 3169.
(51) Kruk, M.; Jaroniec, M.; Kim, J. M.; Ryoo, R. *Langmuir* **1999**, *15*, 5279.
(52) Barrett, E. P.; Joyner, L. G.; Halenda, P. P. *J. Am. Chem. Soc.* **1951**, *73*, 373.
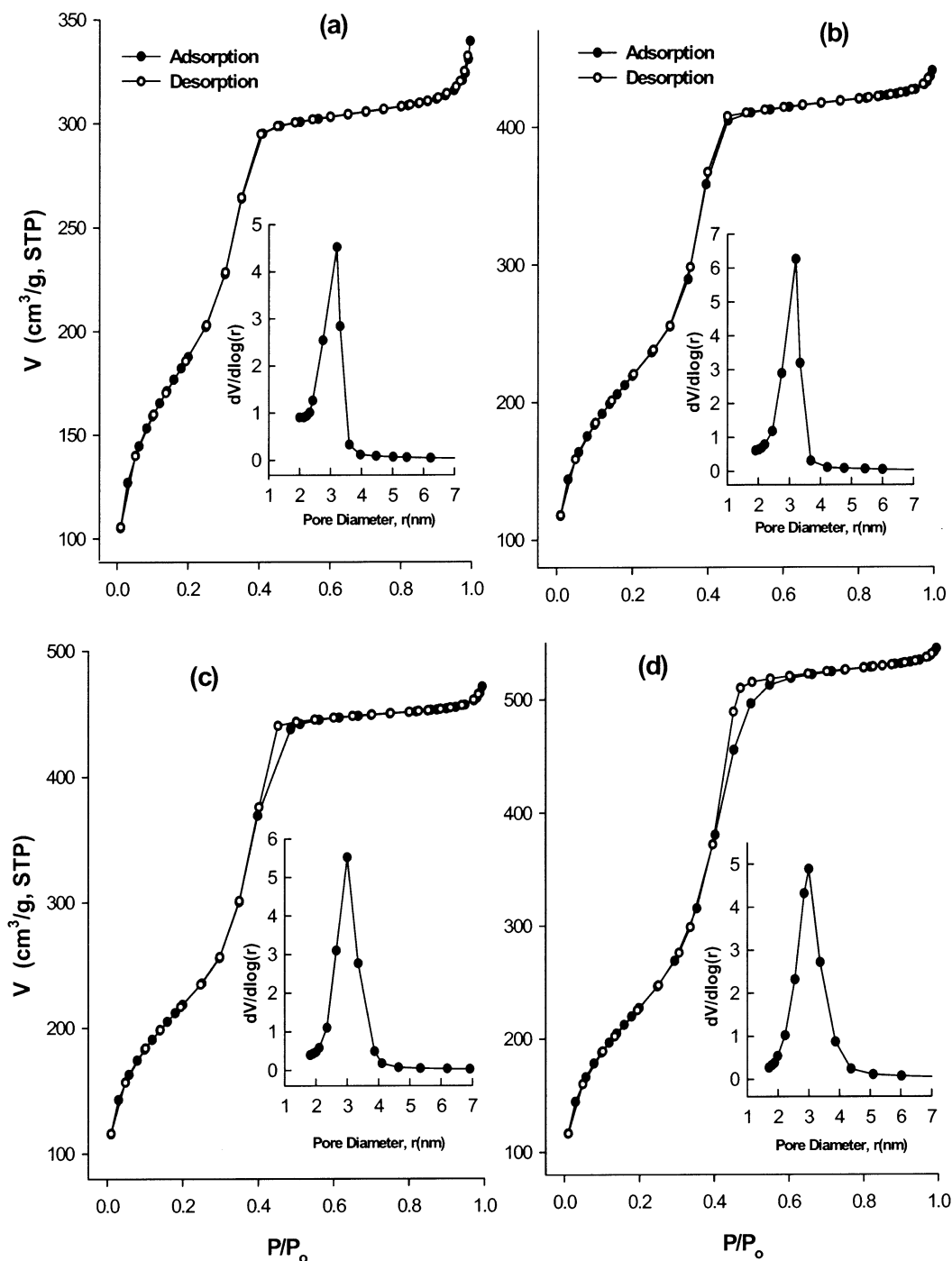
Figure 9. Nitrogen adsorption–desorption isotherms at 77 K of calcined mesoporous silicate and the BJH pore size distribution (inset) for (a) HOM-1 (cubic *Im3m*), (b) HOM-2 (hexagonal *P6mm*), (c) HOM-5 (cubic *Ia3d*), and (d) HOM-7 (cubic *Pn3m*).

size calculated by N_2 sorption isotherms is known to be smaller than the *d* spacing determined by XRD because the latter includes the thickness of the pore wall (*W*). However, *W* is derived from the position of the high-intensity diffraction peaks by the equation $W = [\alpha_o - R]$, where the value of α_o depends on the lattice structure (Table 2). *W* is closely related to the high degree of homogeneity in textural mesoporosity. The large *W* is significantly achieved when the HOM-*n* has high S_{BET} value (Table 2). This result is different from that for MCM-41 synthesized by using CTAB of C_{12}–C_{18} hydrocarbon chain length.[51] Stucky et al. also reported that the large S_{BET} of cubic *Pm3m* and 3-D hexagonal *P6_3/mmc* mesoporous silica films with thicker

W of ca. 10 nm was obtained by using Brij 56 and 76 as structure-directing species.[40] The large *W* of HOM types is characteristic of the high structural stability with the absence of lattice contraction upon calcination.[53]

3. Comparison between HOM-*n* Synthesis by Using Brij 76 and Brij 56 as Templates. It should be noted that the synthesis of mesoporous silica through the direct templating route mainly depends on the phase diagram of surfactant/H_2O systems.[27–32] The binary phase diagram of Brij 76 aggregate was previously observed hexagonal H_I, lamellar L_∞, solid phase (S), and cubic *Ia3d* (V_1) mesophases.[31,33] Also, the phase as-

(53) Zhu, Z.; Chang, Z.; Kevan, L. *J. Phys. Chem. B* **1999**, *103*, 2680.

Table 2. Measured Pore Structural Parameters in the Synthesis of Mesoporous Silicate Monoliths (HOM); Surface Area (S_{BET}), Pore Diameter (R), Total Pore Volume (V), and Wall Thickness (W)

HOM type	mass ratio[a] (%)	S_{BET} (m^2/g)	R (nm)	V (cm^3 g^{-1})	W (nm)
HOM-1	35	690	3.2	0.50	3.4
HOM-2	50	800	3.2	0.67	2.3
HOM-3	69	828	3.5	0.78	5.3
HOM-5	70	832	3.0	0.73	7.3
HOM-6	75	810	3.2	0.78	1.4
HOM-7	85	837	3.0	0.84	7.1
HOM-5[b]	70	789	3.1	0.72	7.5

[a] Brij 56/TMOS concentration ratio (w/w). [b] Solid-phase cubic $Ia3d$ structures.

semblies of Brij 56 contained cubic $Im3m$ (I) more than that obtained with the Brij 76 phase diagram.[29,33] The synthesis methodology of the HOM family using Brij 56 and Brij 76 surfactants reveals that 3-D HOM mesoporous silicates are relatively easier to synthesize by using Brij 56 than by using Brij 76 because they do not require high synthesis temperature and the surfactant concentration ratios used. However, the fabrication of 3-D HOM-n depends on the Brij structure which affects the nature of the Brij surfactant molecules packing of the characteristic geometrical shape of the phase assemblies.[33] Our results suggest that using Brij 56 species significantly enriched the silica mesophases by two unique cubic structures of primitive $Pn3m$ and by bicontinuous S_{Ia3d} symmetry within the similar previously prepared cubic $Ia3d$, cubic $Im3m$, and 3-D hexagonal $P6_3/mmc$ phases by using Brij 76 template. Furthermore, on the basis of the XRD results and on the surface texture data (large S_{BET} and V, as shown in Table 2), all HOM-type silica monoliths fabricated by using Brij 56 species exhibited a higher degree of ordered lattice structures than those fabricated by using Brij 76, consistent with the SBA family synthesized from triblock copolymer surfactants (P123 and P127).[17,18,31] In contrast, the chain length of Brij 56 is expected to lead to well-defined HOM-n structures with lower pore size than that for Brij 76 mesoporous materials.

4. Advantages of HOM-n Synthesis Methodology. In the case of using CTAB-types self-assembly to produce the MCM-like materials, the hydrolysis of silica precursor in a low surfactant concentration leads to the precipitation of the mesoporous silicas as micrometer-sized powders. In this route, the chemical interactions between the cationic surfactant molecules and solvated inorganic silica species (through the charge-density matching across the interfaces) play an important role in determining the topology of the CTAB aqueous domains.[13,14] The absence of sufficiently strong electrostatic or hydrogen-bonding interactions at synthesis conditions leads to the formation of amorphous or

otherwise disordered silica.[22] The resulting materials have a relatively low degree of framework cross-linking and small pore wall thickness. Nevertheless, the pore size of MCM materials is reproducible, but the phase cannot accurately be predicted based only on the starting solution. In contrast, the use of a high concentration of nonionic Brij surfactant permits the pre-existence of the liquid-crystal phases, which directs the formation of the architecture of inorganic mesophase silicates through the true liquid-crystal template mechanism.[27,32] This methodology is a fast, simple method for preparing large monoliths of desired size and shape. However, the formation of porous materials ineffectively depends on the type of interaction and surfactant charge. Therefore, fabrication of not only porous silica but also porous metal is possible. The main advantage of using the lyotropic liquid-crystal template is the predictability of the structure through the higher degree of control over the mesopore organization and surfactant phase domains. A potential advantage of HOM-n silicas produced via templating with Brij surfactant over materials synthesized with cationic surfactants is thicker and has more condensed walls, which improve thermal and mechanical stability of the material.

Conclusion

The formation of large silicate monoliths with a high degree of control over the phase structure and mesopore morphology was creditably achieved, based on our XRD, SEM, and TEM analyses. A lyotropic liquid-crystal template of Brij 56 amphiphile was used to synthesize a well-defined highly ordered mesoporous monolithic family (HOM), including HOM-2 (2-D hexagonal $P6mm$), HOM-6 (lamellar L_∞), HOM-1 (body-centered cubic $Im3m$), HOM-3 (3-D hexagonal $P6_3/mmc$), HOM-5 (cubic solid-phase S_{Ia3d} and normal bicontinuous cubic $Ia3d$), and HOM-7 (primitive-centered cubic $Pn3m$) materials. The synthesis of such bulk mesophases from only one nonionic surfactant established that the direct templating method is a reliable synthetic methodology for the generation of a high-quality mesoscopic morphology. In addition, the HOM synthesis is an easy and simple route for fabricating mesoporous crystalline structures. This periodic mesophase family, HOM, with large caged, uniform mesopore arrays over the long range of all lattice symmetries, with stable wall thickness architectures, and with high crystallinity will be highly valued in applications involving nanoporous materials.